Development/Plasticity/Repair

Requirement of an Allosteric Kinetics of NMDA Receptors for Spike Timing-Dependent Plasticity

Hidetoshi Urakubo,[1] Minoru Honda,[2] Robert C. Froemke,[3] and Shinya Kuroda[1]

[1]CREST, Japan Science and Technology Agency, Department of Biophysics and Biochemistry, Graduate School of Science, University of Tokyo, Bunkyo-ku, Tokyo 113-0033, Japan, [2]Department of Computational Biology, Graduate School of Frontier Sciences, University of Tokyo, Kashiwa 277-8561, Japan, and [3]Department of Molecular and Cellular Biology and Helen Wills Neuroscience Institute, University of California, Berkeley, California 94720-3200

Spike timing-dependent synaptic plasticity (STDP) plays an important role in neural development and information processing in the brain; however, the mechanism by which spike timing information is encoded into STDP remains unclear. Here, we show that a novel allosteric kinetics of NMDA receptors (NMDARs) is required for STDP. We developed a detailed biophysical model of STDP and found that the model required spike timing-dependent distinct suppression of NMDARs by Ca^{2+}-calmodulin. This led us to predict an allosteric kinetics of NMDARs: a slow and rapid suppression of NMDARs by Ca^{2+}-calmodulin with prespiking → postspiking and postspiking → prespiking, respectively. We found that the allosteric kinetics, but not the conventional kinetics, is consistent with specific features of amplitudes and peak time of NMDAR-mediated EPSPs in experiments. We found that the allosteric kinetics of NMDARs was also valid for synaptic plasticity induced by more complex spike trains in layer II/III of visual cortex. We extracted an essential synaptic learning rule by reduction of the allosteric STDP model and found that spike timing-dependent bidirectional role of postspiking in synaptic modification, which depends on the allosteric kinetics, is the essential principle in STDP. Thus, we propose a simple hypothesis of the allosteric kinetics of NMDARs that can coherently explain critical features of spike timing-dependent NMDAR-mediated EPSPs and synaptic plasticity.

Key words: **LTP; LTD; spike timing-dependent plasticity; NMDA receptor; kinetic simulation; systems neurobiology**

Introduction

In the mammalian brain, activity-dependent bidirectional modification of synaptic strength, including long-term potentiation (LTP) and long-term depression (LTD), has been thought to be the molecular and cellular basis of learning and memory (Bi and Poo, 2001). There are various forms of LTP and LTD, but NMDA receptor (NMDAR)-dependent LTP and LTD at excitatory synapses are the most extensively studied and the prototypic form of long-term synaptic plasticity (Malenka and Bear, 2004). The induction of LTP and LTD has been shown recently to depend on the timing between presynaptic and postsynaptic spiking (postspiking), known as spike timing-dependent synaptic plasticity (STDP) (Bi and Poo, 2001; Dan and Poo, 2004). The hallmark of STDP is a spike sequence-dependent bidirectional modification of synaptic strength within a narrow time window between prespiking and postspiking on the order of milliseconds. STDP provides significant computational advantages as a synaptic learning rule, allowing neural circuits to learn temporal sequences of inputs, to shape the temporal and spatial dynamics of neural circuits, and to code causality of external events (Gerstner et al., 1996; Song et al., 2000; Senn, 2002). Additionally, STDP reportedly contributes to the effects of sensory stimuli in the refinement of the retinotectal system *in vivo* (Mu and Poo, 2006; Vislay-Meltzer et al., 2006).

In STDP, prespiking → postspiking is thought to trigger high Ca^{2+} influx via NMDARs and voltage-gated Ca^{2+} channels (VGCCs), which depends on the depolarization-induced removal of the Mg^{2+} block of NMDARs and supralinear summation of EPSPs and backpropagating action potentials (bpAPs) (Hoffman et al., 1997; Stuart and Hausser, 2001; Kampa et al., 2004). The high Ca^{2+} influx is thought to induce activation of Ca^{2+}-calmodulin (CaM)-dependent kinase II (CaMKII), resulting in induction of LTP (Lisman, 1989, 2001; Wang et al., 2005). In contrast, postspiking → prespiking is thought to be mediated by depolarization-dependent suppression of NMDARs (Froemke et al., 2005), which may lead to low Ca^{2+} influx via NMDARs and VGCCs. The low Ca^{2+} influx is thought to induce calcineurin (CaN) activation, resulting in induction of LTD (Lisman, 1989, 2001; Wang et al., 2005). Some forms of LTD in STDP depend on cannabinoid receptor (CB_1)-dependent suppression of transmitter release, in conjunction with activation of presynaptic NMDA autoreceptors (Sjostrom et al., 2003), whereas other forms of LTD do not require CB_1 receptor signaling (Seol et al.,

Received Oct. 19, 2007; accepted Feb. 2, 2008.

This work was supported by a grant-in-aid for scientific research on priority areas "Systems Genomics" (17017005) from the Ministry of Education, Culture, Sports, Science and Technology of Japan and by the Grass Foundation. We thank K. Vance and S. Traynelis for valuable discussions, H. Bito for critically reading this manuscript, and Y. Dan for supporting the experimental portion of this study.

Correspondence should be addressed to either Hidetoshi Urakubo or Shinya Kuroda, Department of Biophysics and Biochemistry, Graduate School of Science, University of Tokyo, Hongo 7-3-1, Bunkyo-ku, Tokyo 113-0033, Japan. E-mail: urakubo@bi.s.u.-tokyo.ac.jp or skuroda@bi.s.u-tokyo.ac.jp.

R. C. Froemke's present address: Department of Otolaryngology, University of California, San Francisco, San Francisco, CA 94143.

DOI:10.1523/JNEUROSCI.0303-08.2008

 0270-6474/08/283310-14$15.00/0

2007). A new study revealed that such controversial results are attributable to different types of neurons or developmental stages (Corlew et al., 2007). Furthermore, recent studies indicate that STDP induction depends not only on the time interval between prespiking and postspiking but also on nonlinear interactions among complex timing prespiking and postspiking (Boettiger and Doupe, 2001; Sjostrom et al., 2001; Froemke and Dan, 2002; Tzounopoulos et al., 2004; Wang et al., 2005; Froemke et al., 2006). Although some phenomenological models have been proposed to describe the interactions among complex timing prespiking and postspiking (Froemke and Dan, 2002; Froemke et al., 2006; Pfister and Gerstner, 2006), the coding mechanism by which spike times are translated into STDP remains unclear because of complexity in signaling mechanisms and properties of STDP.

To address the coding mechanism of STDP, here, we focused on STDP induced in layer II/III lateral connections of visual cortex (Froemke and Dan, 2002; Froemke et al., 2005, 2006) and developed an in-depth biophysical model. We found that spike timing-dependent LTP, but not LTD, could be reproduced. The failure of induction of LTD led us to predict a requirement of slow and rapid suppression of NMDARs by $Ca^{2+} \cdot CaM$ with prespiking → postspiking and postspiking → prespiking, respectively. We found that the predicted allosteric kinetics of NMDARs, but not the conventional kinetics (the binding of glutamate and $Ca^{2+} \cdot CaM$ do not affect their binding to NMDARs each other), appears to be valid for experimental features of NMDAR-mediated EPSPs and for synaptic plasticity induced by more complex spike trains (Froemke and Dan, 2002; Froemke et al., 2006). We extracted an essential synaptic learning rule and found bidirectional regulation of NMDARs by postspiking with allosteric kinetics: the positive regulation of NMDAR activation and Ca^{2+} influx with prespiking → postspiking and the negative regulation of NMDAR activation and Ca^{2+} influx with postspiking → prespiking. We propose that the simple allosteric kinetics of NMDARs is a fundamental coding mechanism for STDP.

Materials and Methods

Development of the STDP model. The STDP model consists of the postsynaptic membrane potential model (see Fig. 1*A*), the postsynaptic signaling cascades model (see Fig. 1*B*), and the AMPA receptors (AMPARs) trafficking model (see Fig. 1*C*). The GENESIS simulator (version 2.2) with a Kinetikit interface was used to numerically simulate spatiotemporal dynamics of electrophysiological and biochemical reactions in the STDP model (Bhalla and Iyengar, 1999). Detailed descriptions of these models, including block diagrams, reactions, and parameters, are described in the supplemental information (http://www.kurodalab.org/info/STDP/Urakubo2008SI.pdf), and the constructed programs are available for download (http://www.kurodalab.org/info/STDP/index.html). Here, a brief overview of the STDP model is presented as follows.

Modeling of postsynaptic neuron. We constructed a multicompartment model of a postsynaptic neuron with Hodgkin–Huxley-like channel kinetics on the basis of the previous models (see Fig. 1*A*) (Migliore et al., 1999; Poirazi et al., 2003). The model has one somatic and 20 dendritic compartments (see Fig. 1*A*), which incorporate spike-generating Na^+ channels, persistent Na^+ channels, delayed rectifier K^+ channels, A-type K^+ channels, and L-type VGCCs with spatially inhomogeneous densities. The synaptic site is assumed to be 60 μm apart from the soma (third dendritic compartment from the soma). Presynaptic stimulation leads to probabilistic release of glutamate from presynaptic terminals, which activates postsynaptic AMPARs and NMDARs. Postsynaptic stimulation (current injection) elicits APs.

Modeling of postsynaptic signaling cascades. We modeled Ca^{2+} influx to a spine via NMDARs and VGCCs, as well as Ca^{2+} uptake from the spine, and simulated postsynaptic Ca^{2+} concentration $[Ca^{2+}]_{PSD}$ in response to presynaptic and postsynaptic stimulation on the basis of the previous observations (see Fig. 1*B*) (Sabatini et al., 2001). We also modeled intracellular signaling cascades within the spine on the basis of the previous models (Bhalla and Iyengar, 1999; Kuroda et al., 2001; Doi et al., 2005) and observations (Winder and Sweatt, 2001; Lisman et al., 2002). The spine is divided into cytosol and postsynaptic density (PSD) compartments. We incorporated interactions among Ca^{2+}, CaM, CaMKII, CaN, protein kinase A (PKA), adenylnyl cylase 1/8 (AC1/8), cAMP, phosphorylated inhibitor-I (I-1), protein phosphatase 1 (PP1), and protein phosphatase 2A (PP2A). The molecules diffuse between the cytosol and PSD compartments, where CaMKII, PP1, and PP2A interact with scaffold (cytoskeletal scaffolds). We assumed that the molecules within each compartment are well mixed, and that they deterministically interact on the basis of mass assumption.

Modeling of AMPAR trafficking. We constructed a simplified model of phosphorylation-dependent AMPAR [glutamate receptor 1 (GluR1)] trafficking on the basis of the previous experiments (see Fig. 1*C*) (Malinow and Malenka, 2002; Collingridge et al., 2004; Seol et al., 2007). An AMPAR subunit, GluR1, is phosphorylated by PKA at Ser845, and PDZ (PSD-95/Discs large/zona occludens-1)-containing proteins, which associate AMPARs, are phosphorylated by CaMKII. AMPARs are involved in the following recycling processes: (1) AMPARs with phosphorylated PDZs are trapped by scaffold at PSD fraction, (2) AMPARs are diffused laterally in the membrane, and (3) dephosphorylated AMPARs (GluR1 s at Ser845) are internalized by endocytosis, and phosphorylated AMPARs are reinserted into the membrane via exocytosis. We assumed that AMPAR number trapping at scaffolds of PSD corresponds to synaptic conductance.

Electrophysiology. Acute visual cortical slices were prepared from 2- to 4-week-old Sprague Dawley rats. Somatic whole-cell recordings were made from layer II/III pyramidal cells in current-clamp mode. EPSPs were evoked by focal extracellular stimulation, and postsynaptic APs were elicited with current injection through the recording electrode. Synaptic strength was measured as the initial 2 ms slope of the EPSP at 11–20 min after the end of induction. The detailed experimental procedures are described previously (Froemke and Dan, 2002; Froemke et al., 2005, 2006).

Results

Development of the STDP model

To understand the mechanism of spike-timing detection in STDP, we developed a realistic biophysical model of synaptic plasticity within a single postsynaptic spine, on the basis of the literature and recent experimental findings on ion channels, intracellular signaling cascades, and receptor trafficking (Fig. 1*A–C*) (supplemental information, http://www.kurodalab.org/info/STDP/Urakubo2008SI.pdf). In this model, prespiking and postspiking are inputs, and the change of synaptic conductance is the output. Prespiking represents glutamate release from the presynaptic terminal, which involves short-term depression of transmitter release probability during high-frequency bursts (>2 Hz) (Tsodyks and Markram, 1997; Matveev and Wang, 2000; Froemke et al., 2006). The postspiking signal is a large increase of membrane potential via bpAPs (Hoffman et al., 1997; Stuart and Hausser, 2001), which involves frequency-dependent attenuation (Froemke et al., 2006). We used 1 Hz prespiking for 100 s over a range of constant membrane potentials, which corresponds to the postspiking signal (Artola et al., 1990; Feldman, 2000; Lisman, 2001; Stiefel et al., 2005), as test stimuli to constrain the electrophysiological and biochemical dynamics of the STDP model (Fig. 2).

At membrane potentials positive from −45 mV, the Mg^{2+} block of NMDARs was removed, and the high Ca^{2+} influx via NMDARs (Fig. 2*A*,*F*) produced sufficient $Ca^{2+} \cdot CaM$. This then bound to each subunit of a holoenzyme of CaMKII and

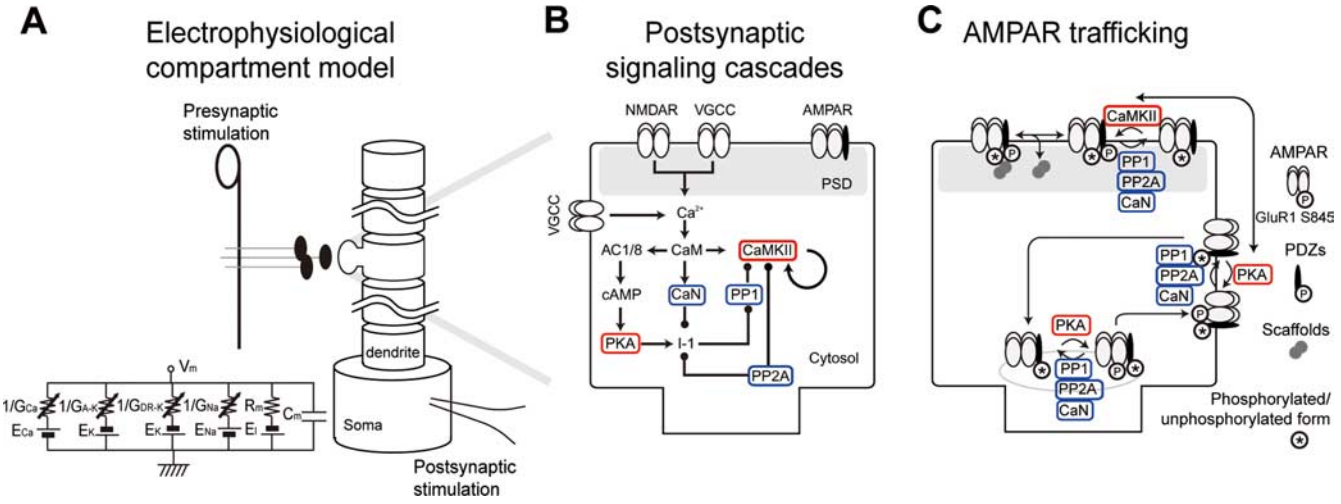

Figure 1. Development of the STDP model. ***A***, Electrophysiological compartment model. ***B***, Postsynaptic signaling cascades model, which includes Ca^{2+} influx and removal and biochemical interactions. ***C***, AMPAR trafficking model. The arrows and lines with a black circle indicate stimulatory and inhibitory interactions, respectively. Molecules required for LTP and LTD are indicated by red and blue, respectively. The detailed description of the models is provided as supplemental information (available at http://www.kurodalab.org/info/STDP/Urakubo2008SI.pdf).

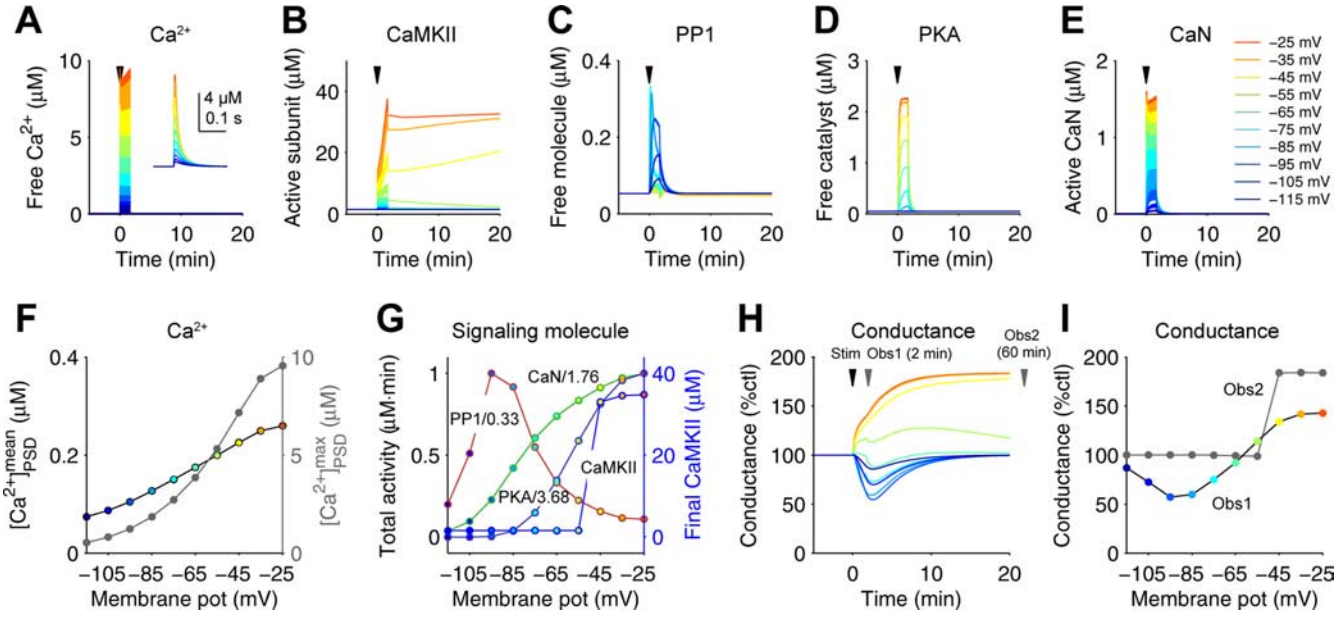

Figure 2. Voltage-dependent changes of synaptic strength. ***A–E***, Time courses of Ca^{2+} concentration (***A***), CaMKII activity (***B***), PP1 activity (***C***), PKA activity (***D***), and CaN activity (***E***) at PSD in response to 100 prespikes at 1 Hz with the indicated voltage clamp of somatic membrane potential during the stimulation. Colors correspond to the voltage as indicated in ***E***. Arrowheads indicate the onset of stimulation. The inset in ***A*** shows its time courses by a single prespiking. ***F***, Voltage-dependent Ca^{2+} concentration at PSD. The black and gray lines indicate the mean and maximal amplitude of Ca^{2+} concentration, respectively. ***G***, Voltage-dependent CaN, PKA, PP1, and CaMKII activities. Integrated PP1 activity (red; normalized with the maximal activity, 0.33), integrated PKA activity (dark blue; normalized by 3.68), integrated CaN activity (green; normalized by 1.75), and final CaMKII activity (light blue) against the indicated membrane potentials are plotted. ***H***, Time courses of changes of synaptic conductance. ***I***, Voltage-dependent changes of synaptic conductance. Data were taken at 2 and 60 min after the onset of stimulation (Obs 1 and Obs 2, respectively) as indicated in ***H***.

induced successive autophosphorylation of CaMKII subunits, which led to the persistent activation of CaMKII (Fig. 2*B*,*G*) (Lisman et al., 2002). The persistent CaMKII activation required the inhibition of PP1 activity (Fig. 2*C*,*G*), which dephosphorylates CaMKII. The high Ca^{2+} influx also activated PKA via AC1/8 (Fig. 2*D*,*G*) and CaN (Fig. 2*E*,*G*). PP1 was inactivated by phosphorylated I-1, the dephosphorylation and phosphorylation of which depend on CaN and PKA, respectively. The high Ca^{2+} influx inhibited PP1 via phosphorylated I-1, because its phosphorylation by PKA counteracts with dephosphorylation by CaN (Figs. 1*B*, 2*D*,*E*,*G*). Therefore, PKA activation is necessary to trigger the persistent CaMKII activation via inhibition of PP1, which is consistent with the observation that PKA acts as a gate signal for LTP induction (Blitzer et al., 1998).

In contrast, at hyperpolarized membrane potentials such as −85 mV, the low Ca^{2+} influx (Fig. 2*A*,*F*) also produced Ca^{2+} · CaM; however, this activated CaN without sufficient activation of PKA and CaMKII (Fig. 2*G*), and the activated CaN dephosphorylated I-1 and activated PP1 (Fig. 2*C*,*E*,*G*) (Winder and Sweatt, 2001). Therefore, the low Ca^{2+} influx specifically induced activation of protein phosphatases rather than of protein kinases, consistent with previous observations (Bear and Malenka, 1994). The sensitivities to Ca^{2+} influx between protein phosphatases and kinases were attributable to the distinct sensi-

tivities of CaN and PKA to $Ca^{2+} \cdot CaM$ (Fig. 2*G*). However, in contrast to CaMKII activation, PP1 activation was transient and returned to basal levels after stimulation (Fig. 2*C*).

The specific activation of signaling molecules regulated trafficking of AMPARs and thus regulated AMPAR synaptic conductance (Figs. 1*C*, 2*H*) (Malinow and Malenka, 2002; Collingridge et al., 2004; Seol et al., 2007). Persistent activation of CaMKII phosphorylated PDZs, including synapse-associated protein 97 and stargazin. The phosphorylation facilitated AMPAR trapping by cytoskeletal scaffolds (scaffolds) at PSD (Fig. 1*C*) and resulted in a persistent increase of AMPARs at PSD and of conductance, resulting in expression of LTP (Fig. 2*H*). Note that the persistent CaMKII activation was the only stabilizing mechanism for LTP and that no other stabilizing mechanisms, such as protein synthesis and AMPAR clustering, were modeled in this study. In contrast, both PP1 and CaN dephosphorylated PDZs and GluR1 at Ser845 (a subunit of AMPARs). Dephosphorylation of PDZs and GluR1 at Ser845 resulted in the dissociation of AMPARs from PSD and facilitated the internalization of AMPARs into the endosome, respectively (Fig. 1*C*). The internalized AMPARs were maintained in the dephosphorylated state by the action of PP1 and CaN, which prevented the AMPARs from being reinserted, and resulted in a decrease of conductance through AMPAR channels (Fig. 2*H*). However, because the activation of CaN and PP1 was transient, the number of AMPARs within the PSD and, correspondingly, the total prespike-evoked synaptic conductance eventually returned to the basal level. This result indicates that the stabilization of LTD cannot be explained with the experimentally observed time constants of AMPAR trafficking and suggests the presence of an unidentified pathway or pathways that are responsible for the maintenance of LTD. The mechanisms of persistency for LTD remain unknown; however, the saturation-dependent trafficking of AMPARs (Hayer and Bhalla, 2005) or the clustering of interacting receptors (Shouval, 2005) may be possible mechanisms. Although depression was not persistent, short-term, voltage-dependent changes of synaptic strength in our model were highly correlated with depolarization-dependent LTP and hyperpolarization-dependent LTD observed experimentally (Fig. 2*I*) (Artola et al., 1990; Stiefel et al., 2005). Similarly, we experimentally found that, by use of pharmacological manipulation, high, moderate, and low NMDAR activities are correlated with potentiation, no change (neither potentiation nor depression), and depression, respectively (supplemental Fig. 1, available at www.jneurosci.org as supplemental material). Because the NMDAR activity depends on the membrane potential, this result is consistent with synaptic plasticity induced by direct depolarization (Malenka and Bear, 2004). Therefore, we confirmed that our STDP model is, in principle, consistent with membrane potential-dependent synaptic plasticity and with related molecular events.

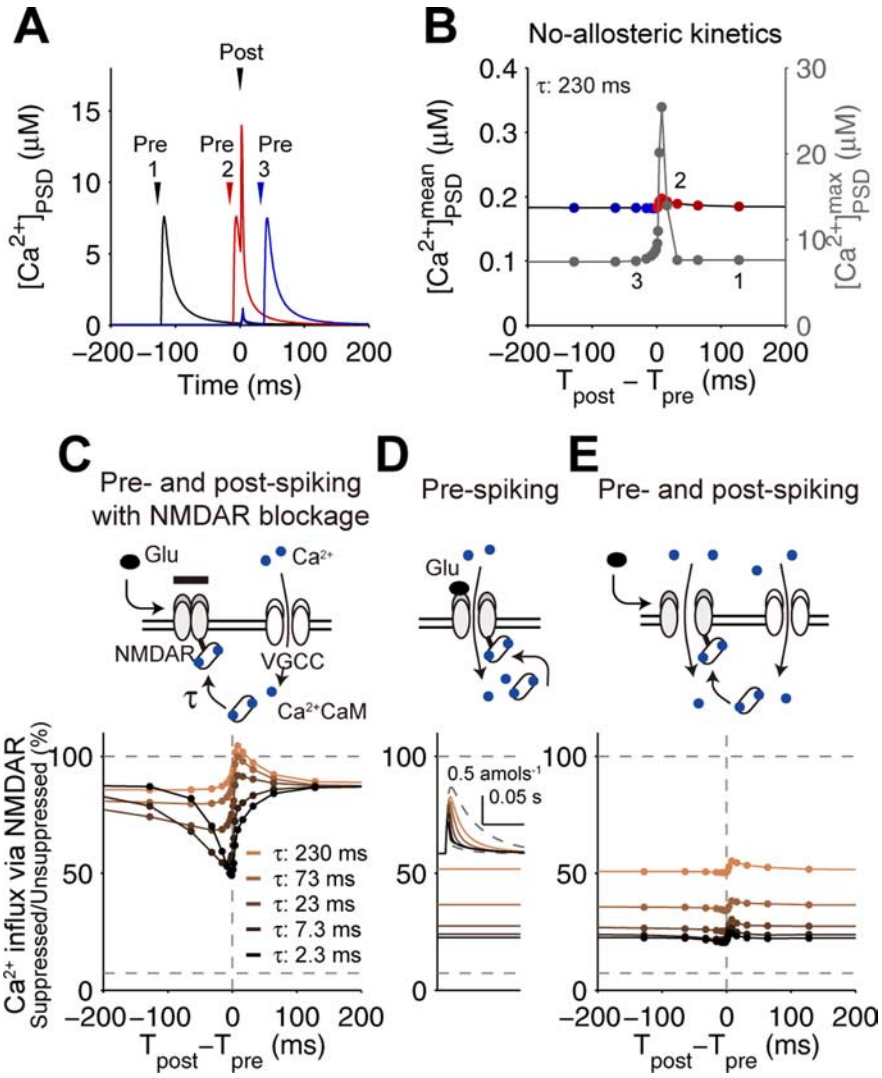

Figure 3. Requirement of the distinct suppression of NMDARs. ***A***, Time courses of spike timing-dependent $[Ca^{2+}]_{PSD}$ by a single pairing of prespiking and postspiking in the STDP model (the no-allosteric model) with the indicated spike timing in ***B***; 1, prespiking → postspiking ($T_{post} - T_{pre} = +128$ ms; black); 2, prespiking → postspiking (+16 ms; red); 3, postspiking → prespiking (−32 ms; blue). ***B***, Spike timing-dependent Ca^{2+} increase in the no-allosteric model. The mean and maximum $[Ca^{2+}]_{PSD}$ are indicated by black and gray, respectively. The mean denotes the integration of Ca^{2+} induced by a single pairing of prespiking and postspiking divided by 1 s. T_{post} was defined as the time of 5 ms after the onset of current injection represented by an α-function (500 pA, 0.5 ms), and T_{pre} was defined as the time of the onset of glutamate release. The positive (red) and negative (blue) intervals correspond to the prespike → postspike and postspike → prespike timing, respectively. ***C***, Spike timing-dependent suppression of NMDARs under the blockage of Ca^{2+} influx via NMDARs. Expected Ca^{2+} influx, if the NMDARs open, are plotted with the indicated time constant of $Ca^{2+} \cdot CaM$ binding to NMDARs, τ. Ca^{2+} influx via NMDARs was normalized by unsuppressed Ca^{2+} influx (***C–E***). ***D***, Ca^{2+} influx via NMDARs induced by a prespiking alone with the indicated τ. The inset shows the time courses of the total NMDAR-mediated Ca^{2+} influx. ***E***, Spike timing-dependent Ca^{2+} influx via NMDARs.

Prediction of the allosteric kinetics of NMDARs

We next explored whether the experimentally determined dynamics of STDP can be reproduced in our biophysical model. We used a brief current injection to the somatic compartment to trigger postspiking and bpAPs within the spine. Neither prespiking nor postspiking with 1 Hz for 100 s alone induced synaptic plasticity (see Fig. 4*E*) (Johnston et al., 2003). Induction of LTP

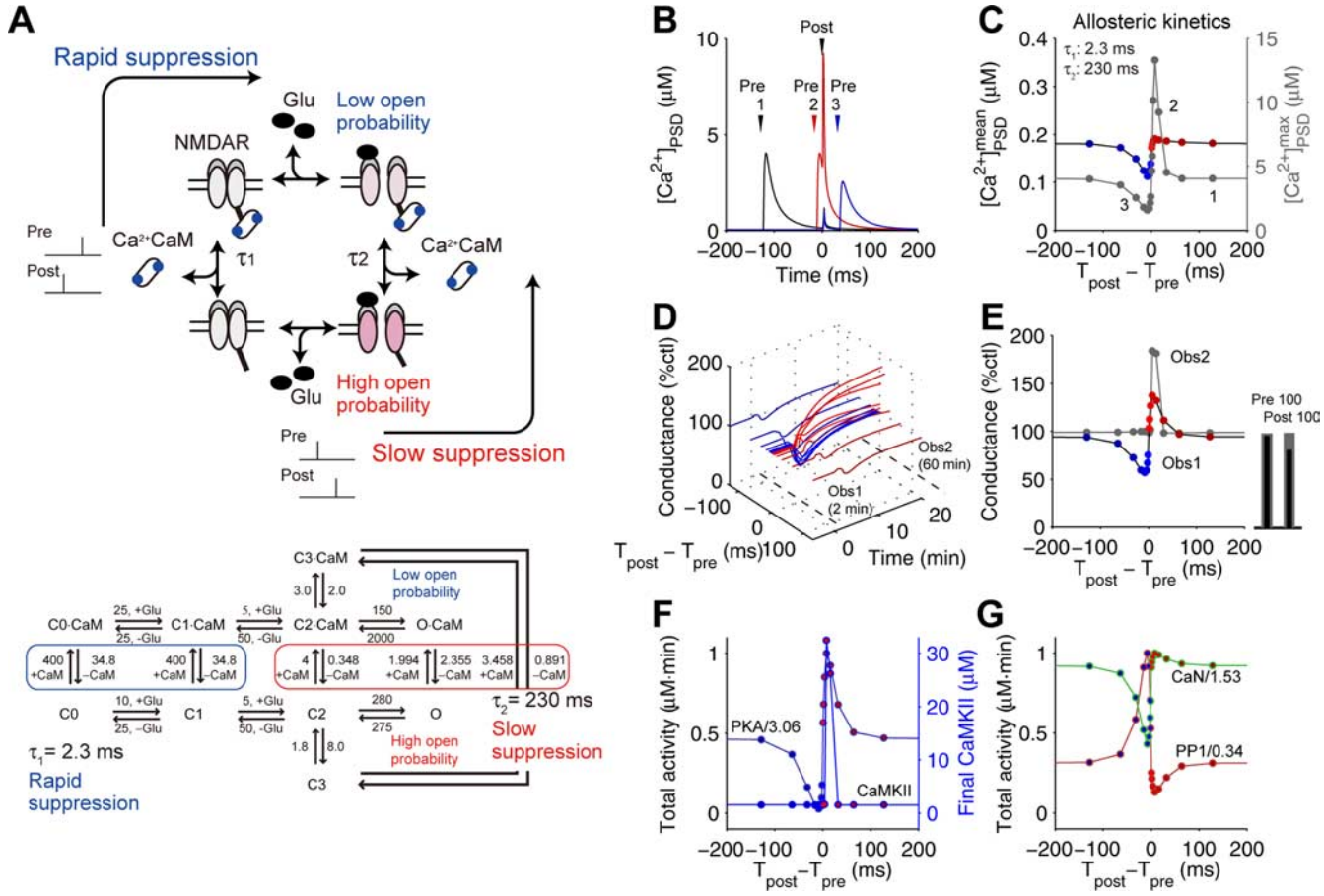

Figure 4. Prediction of the allosteric kinetics of NMDARs. ***A***, Schematic (top) and detailed mechanism (bottom) of the allosteric kinetics of NMDARs. τ_1 and τ_2 were the time constants of Ca^{2+} · CaM binding to glutamate (Glu)-unbound and Glu-bound NMDARs, respectively, where Ca^{2+} · CaM concentration is 1 μM. Ca^{2+} · CaM bound and Ca^{2+} · CaM unbound NMDARs, which bind to Glu, show the low and high open probability, respectively (Ehlers et al., 1996; Rycroft and Gibb, 2002, 2004b). C_0, C_1, C_2, C_3, C_0 · CaM, C_1 · CaM, C_2 · CaM, and C_3 · CaM are the concentrations of closed-state NMDARs, and *O* and *O* · CaM are those of open-state NMDARs (bottom). CaM represents 2 Ca^{2+} · CaM or 3 Ca^{2+} · CaM, and the numerals on arrows are rate constants in $\mu M^{-1}s^{-1}$ or s^{-1}, which were set on the basis of the experimental observation (bottom). The complete description of the allosteric kinetics of NMDARs is provided on-line (available at http://www.kurodalab.org/info/STDP/Urakubo2008SI.pdf). ***B***, Time courses of spike timing-dependent $[Ca^{2+}]_{PSD}$ by a single pairing of prespiking and postspiking in the allosteric model with the indicated spike timing in ***C***. ***C***, Spike timing-dependent $[Ca^{2+}]_{PSD}$ in the allosteric model with the indicated τ_1 and τ_2. ***D***, Time courses of spike timing-dependent synaptic conductance in the allosteric model. One hundred pairings of the prespiking and postspiking with 1 Hz were given. ***E***, Spike timing-dependent synaptic conductance in the allosteric model at 2 min (Obs 1) and 60 min (Obs 2) after the onset of stimulation (left). The apparent time constants for LTP and LTD at 2 min were 36.1 and 53.0 ms, respectively. The synaptic conductance with 100 prespikes and postspikes alone at 2 min (black) and 60 min (gray) after the onset of stimulation is also plotted (right, bars). ***F***, Integrated PKA activity (normalized by 3.06) and final CaMKII activity. ***G***, Integrated PP1 activity (normalized by 0.34) and integrated CaN activity (normalized by 1.53).

by prespiking → postspiking is thought to be triggered by accelerated Ca^{2+} influx via NMDARs and VGCCs, which depends on the depolarization-induced removal of the Mg^{2+} block of NMDARs and supralinear summation of EPSPs and bpAPs (Hoffman et al., 1997; Stuart and Hausser, 2001; Kampa et al., 2004). Induction of LTD by postspiking → prespiking has been shown recently to be mediated by depolarization-dependent suppression of NMDARs (Froemke et al., 2005), which may lead to reduced Ca^{2+} influx through NMDARs and VGCCs. Moreover, the direct binding of Ca^{2+} · CaM to NMDARs reduces mean open time and leads to an overall reduction of open probability, resulting in suppression of NMDARs (Ehlers et al., 1996; Rycroft and Gibb, 2002, 2004b). Therefore, we first examined whether accelerated or suppressed Ca^{2+} influx can be induced by prespiking → postspiking or postspiking → prespiking via NMDARs, respectively (Fig. 3). Prespiking → postspiking led to accelerated Ca^{2+} influx via bpAP-dependent removal of the Mg^{2+} block of NMDARs (Fig. 3*A*,*B*), which led to induction of LTP (supplemental Fig. 2, available at www.jneurosci.org as supplemental material). However, postspiking → prespiking did not suppress Ca^{2+} influx (Fig. 3*A*,*B*), in contrast to the experimental evidence (Froemke et al., 2005), and did not induce LTD (supplemental Fig. 2, available at www.jneurosci.org as supplemental material). This result indicates the existence of an unknown mechanism for suppression of Ca^{2+} influx.

The failure to suppress Ca^{2+} influx by postspiking → prespiking led us to examine the mechanism of suppression of NMDARs by Ca^{2+} · CaM. We changed the time constant of Ca^{2+} · CaM binding to NMDARs under the blockage of NMDAR-dependent Ca^{2+} influx and examined the suppression of NMDARs solely by VGCC-dependent Ca^{2+} influx, which is triggered by postspiking (Fig. 3*C*). NMDARs were suppressed by VGCC-dependent Ca^{2+} influx with the rapid time constant (2.3 ms) but not with the slow time constant (230 ms). This indicates that suppression of NMDARs by VGCC-dependent Ca^{2+} influx, which may reflect the time window for LTD induction with postspike → prespike timing (Froemke et al., 2005), requires a rapid binding of Ca^{2+} · CaM to NMDARs. We also examined suppression of NMDARs by NMDAR-dependent Ca^{2+} influx induced by prespiking alone (Fig. 3*D*). Ca^{2+} influx was gradually reduced as the

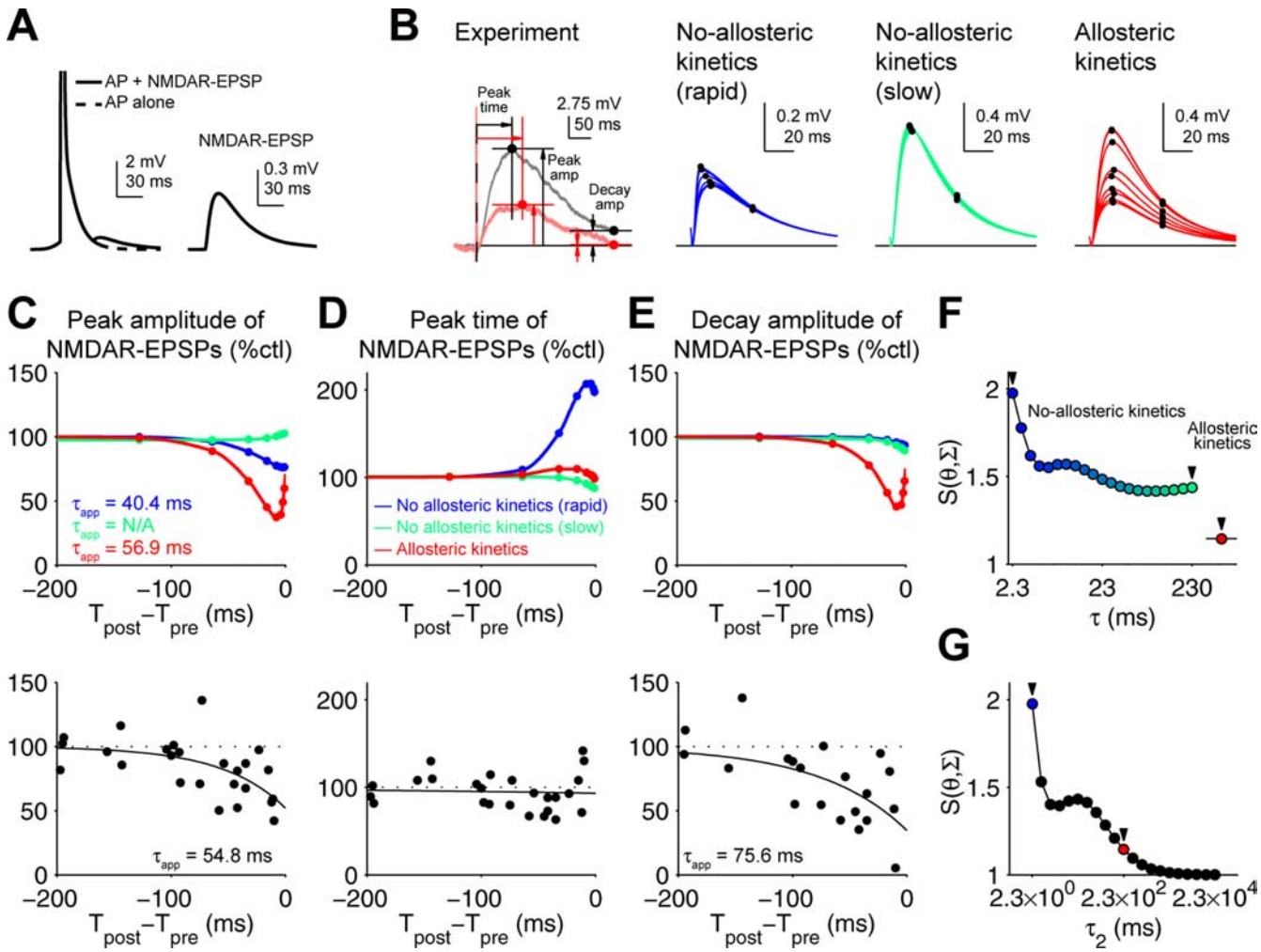

Figure 5. Features of the allosteric kinetics in NMDAR-EPSP. ***A***, Derivation of NMDAR-EPSPs by postspiking ⟶ prespiking. NMDAR-EPSPs (right) was derived by the subtraction of AP alone from the NMDAR-EPSP plus AP in the absence of AMPAR activation (left, solid line) in presence of CNQX, a specific AMPAR antagonist (Froemke et al., 2005) (left, dashed line). ***B***, Time courses of NMDAR-EPSPs by postspiking ⟶ prespiking in experiment ($T_{post} - T_{pre} = -10$ ms, red; prespike-only as control, gray), in the no-allosteric model ($-1, -2, -4, \ldots, -256$ ms) with rapid ($\tau_1 = \tau_2 = 2.3$ ms) and slow ($\tau_1 = \tau_2 = 230$ ms) suppression, and in the allosteric model ($-1, -2, -4, \ldots, -256$ ms; $\tau_1 = 2.3$ ms and $\tau_2 = 230$ ms), as indicated. ***C–E***, Peak amplitude (***C***), peak time (***D***), and decay amplitude (***E***) of NMDAR-EPSPs in the models (top) and the experiments (bottom). The responses were normalized by the control responses. The decay amplitude was taken at the time when three times longer than the largest peak time in each set. The responses of the no-allosteric model with rapid and slow suppression (blue and green, respectively) and the allosteric model (red) are plotted (top). The timing-dependent NMDAR-EPSPs in the experiments were fitted by a single exponential curve using the least square method (bottom). The apparent time constants of the responses of NMDAR-EPSPs versus the spike timing, τ_{app}, are indicated. ***F***, Evaluation of goodness of fit of the no-allosteric and allosteric models with the experimental data. The time constant in the no-allosteric model was changed as indicated, and the measure $S(\theta, \Sigma)$ was plotted. $S(\theta, \Sigma)$ is a sum of variance and covariance of errors between experiment and simulation in peak amplitude, peak time, and decay amplitude, normalized by variance and covariance of residuals in the best-fit model. $S(\theta, \Sigma)$ is given by $S(\theta,\Sigma) = [3(n-1)]^{-1}\sum_{i=1}^{n}[Y_i - f(x_i,\theta)]^t\Sigma^{-1}[Y_i - f(x_i,\theta)]$, where $f(x_i, \theta)$ is the fitting function, and θ is the parameter vector, Σ is the variance– covariance matrix of residuals of the best-fit model ($\tau_1 = 2.3$ ms and $\tau_2 = 2.3 \times 10^4$ ms), Y_i is a column vector of the peak amplitude, peak time, and decay amplitude of ith NMDAR-EPSP, and x_i is $T_{post} - T_{pre}$ of the EPSP (Gallant, 1987). Note that the closer to 1 the $S(\theta, \Sigma)$ becomes, the better the model fits the experimental results. Arrowheads denote the time constants used in the no-allosteric and allosteric models. ***G***, Goodness of fit against various time constant of Ca^{2+} · CaM binding to NMDARs, τ_2, in the allosteric model. The τ_2 was changed as indicated, and the $S(\theta, \Sigma)$ was measured. The arrowhead indicates τ_2 (230 ms) used in the allosteric model.

time constant of Ca^{2+} · CaM binding to NMDARs became rapid because of the self-suppression of NMDARs by Ca^{2+} influx through themselves. This indicates that the slow binding of Ca^{2+} · CaM to NMDARs is required to avoid self-suppression of NMDARs. We examined the suppression of NMDARs by both NMDAR- and VGCC-dependent Ca^{2+} influx and found that suppression of NMDARs did not change regardless of spike timing with any time constant and resulted in a failure of spike-timing detection (Fig. 3*E*). This result indicates that, with postspike ⟶ prespike timing, a rapid binding of Ca^{2+} · CaM to NMDARs is required to suppress NMDARs by VGCC-dependent Ca^{2+} influx, whereas with prespike ⟶ postspike timing, a slow binding of Ca^{2+} · CaM to NMDARs is required to avoid the rapid self-suppression of NMDARs.

This requirement of distinct suppression of NMDARs in a spike timing-dependent manner led us to predict an allosteric kinetics of NMDARs: rapid binding of Ca^{2+} · CaM to glutamate-unbound NMDARs and slow binding of Ca^{2+} · CaM to glutamate-bound NMDARs (Fig. 4*A*) (supplemental information, available at http://www.kurodalab.org/info/STDP/Urakubo2008SI.pdf). For simplicity, we changed the association and dissociation time constants without changing the affinity of Ca^{2+} · CaM to NMDARs. Hereafter, the STDP model (with or without the allosteric kinetics of NMDARs) denotes the allosteric

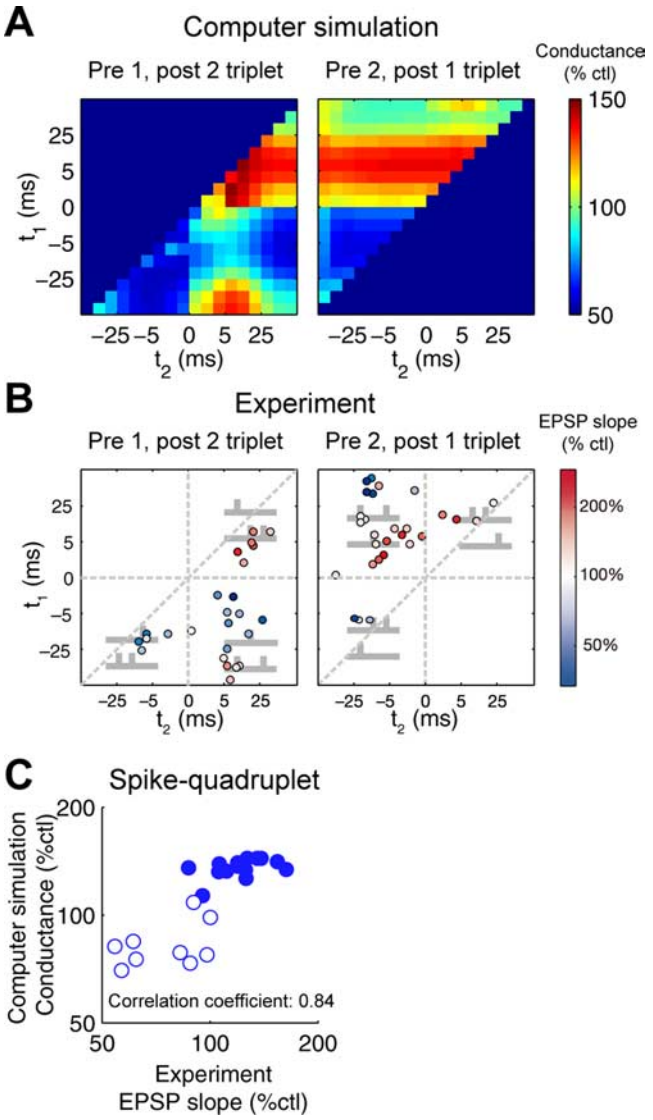

Figure 6. Complex spike timing-dependent synaptic plasticity. ***A***, ***B***, Changes of synaptic strength by spike triplets in the allosteric model (***A***) and in the experiments (***B***) (Froemke and Dan, 2002) (reproduced with permission from *Nature*). One prespiking and two postspiking (left), where t_1 indicates the relative timing of the first postspiking to prespiking ($T_{post\,1} - T_{pre}$), and t_2 indicates the relative timing of the second postspiking to prespiking ($T_{post\,2} - T_{pre}$). Two prespiking and one postspiking (right), where $t_1 = T_{post} - T_{pre\,1}$ ($T_{pre\,1}$, first prespiking) and $t_2 = T_{post} - T_{pre\,2}$ ($T_{pre\,2}$, second prespiking). Data in ***A*** were taken at 2 min after onsets of stimulation and averaged across three trials with different profiles of glutamate release based on presynaptic short-term depression (SEM $<$0.26%). ***C***, Changes of synaptic strength by spike quadruplets. Synaptic conductance in the allosteric model versus correspondence in the experiments was plotted (Froemke et al., 2005). Open symbols, Prespiking → postspiking → postspiking → prespiking; filled symbols, postspiking → prespiking → prespiking → postspiking. Simulation data were averaged across three trials (SEM $<$0.38%).

or no-allosteric model, respectively. The allosteric model led to suppression of Ca^{2+} influx with postspike → prespike timing and accelerated Ca^{2+} influx with prespike → postspike timing (Fig. 4*B*,*C*), resulting in STDP (Fig. 4*D*,*E*), although any no-allosteric model with rapid or slow binding of Ca^{2+} · CaM to NMDARs did not produce the appropriate Ca^{2+} influx and subsequent STDP (supplemental Fig. 2, available at www.jneurosci.org as supplemental material). Note that the curve in LTP at 2 min was graded, but it became bistable at 60 min. Such slow increase is one of the unusual properties of spike timing-dependent LTP observed in experiments (Bi and Rubin, 2005).

In the allosteric model, accelerated Ca^{2+} influx with prespike → postspike timing specifically induced CaMKII and PKA activation and PP1 suppression (Fig. 4*F*,*G*), which induced LTP (Fig. 4*D*,*E*). Persistent CaMKII activation requires a suprathreshold Ca^{2+} influx because of the nature of its autophosphorylation loop, so the high Ca^{2+} influx, rather than the low and sustained Ca^{2+} influx, preferentially triggers CaMKII activation and subsequent LTP induction (Fig. 4*C*,*E*,*F*) (supplemental Fig. 2, available at www.jneurosci.org as supplemental material). In contrast, suppressed Ca^{2+} influx with postspike → prespike timing specifically induced PP1 activation without PKA activation (Fig. 4*C*,*F*,*G*), which induced LTD (Fig. 4*D*,*E*). Because PKA was not fully activated by the suppressed Ca^{2+} influx (Fig. 2*G*), PP1 activity was not suppressed and exhibited the highest activity at the low Ca^{2+} level (Fig. 2*G*). Also, because the PP1 activation has several steps from Ca^{2+}, the PP1 activation requires enough duration of Ca^{2+}. Therefore, the low and sustained Ca^{2+} influx, rather than the high and transient Ca^{2+} influx, preferentially induces LTD (Fig. 4*C*,*E*,*G*; supplemental Fig. 2, available at www.jneurosci.org as supplemental material). These results indicate that the allosteric kinetics of NMDARs can reliably detect prespike and postspike timing, which lead to STDP.

Features of the allosteric kinetics of NMDARs

To test the prediction of the allosteric kinetics of NMDARs, we measured the NMDAR-mediated EPSPs (NMDAR-EPSPs), which should directly show the effect of the allosteric kinetics, under the conditions where any component of AMPAR-EPSPs was not involved (Fig. 5*A*). We compared the amplitudes and time of NMDAR-EPSPs between the models and the experiments (Fig. 5*B*). In the allosteric model, the peak amplitudes of the NMDAR-EPSPs decreased with postspike → prespike timing (Fig. 5*C*, top). The peak amplitudes of the NMDAR-EPSPs in the no-allosteric model with rapid suppression (τ = 2.3 ms) also slightly decreased; however, those with slower suppression (τ = 230 ms) did not decrease with postspike → prespike timing (Fig. 5*C*, top). Experimentally, the peak amplitudes of the NMDAR-EPSPs also decreased (Fig. 5*C*, bottom). This experimental result is consistent with the results of both the allosteric model and the no-allosteric model with rapid suppression. We then compared the peak time of NMDAR-EPSPs (Fig. 5*D*). In the allosteric model and the no-allosteric model with slow suppression, the peak time of the NMDAR-EPSPs remained constant regardless of the spike timing, whereas the peak time of the NMDAR-EPSPs in the no-allosteric model with rapid suppression was delayed with postspike → prespike timing, because the decay of NMDAR-EPSPs is suppressed by Ca^{2+} influx via NMDARs themselves (Fig. 5*D*, top). In the experiments, the peak time of the NMDAR-EPSPs was not delayed and remained constant (Fig. 5*D*, bottom). This experimental result is consistent with the results in the allosteric model and in the no-allosteric model with slow suppression. We further examined the amplitude at the decay phase (decay amplitude), because the effect of the allosteric kinetics can appear more clearly during the decay phase. The decay amplitudes of the NMDAR-EPSPs in the allosteric model decreased; however, those in the no-allosteric models did not decrease with postspike → prespike timing (Fig. 5*E*, top). Experimentally, the decay amplitudes of the NMDAR-EPSPs also decreased (Fig. 5*E*, bottom). This exper-

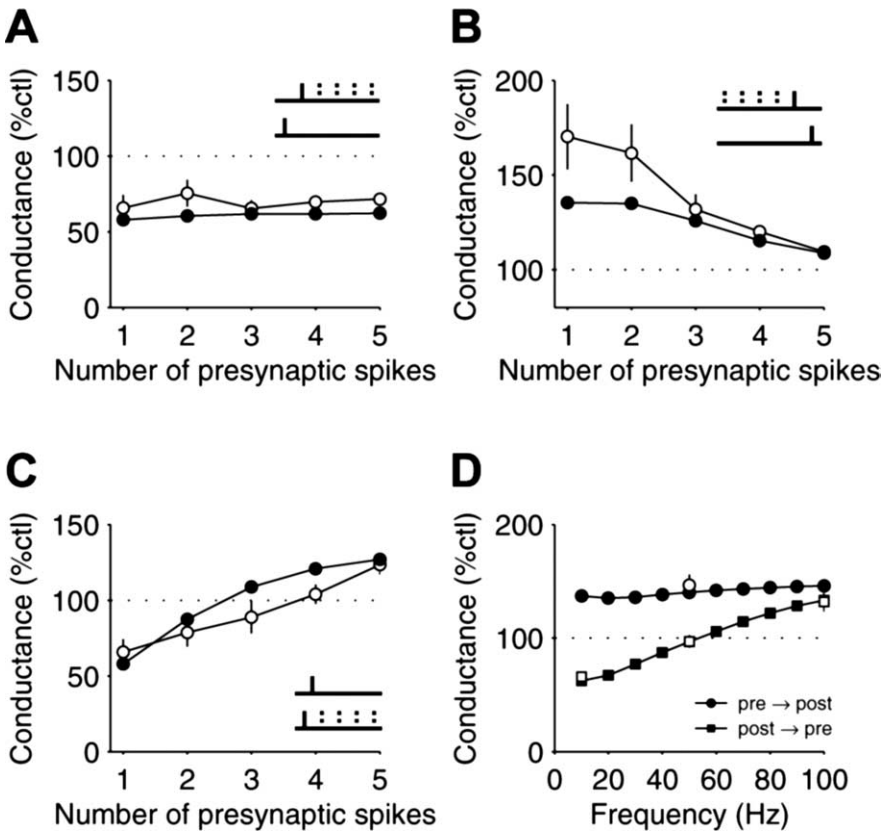

Figure 7. Burst-dependent synaptic plasticity. ***A***, ***B***, Changes of synaptic strength by presynaptic bursts with a single postsynaptic spike. The presynaptic spikes (with the indicated numbers) with 100 Hz after (***A***) or before (***B***) a postsynaptic spike was given at 1 Hz for 100 times. The interval between the postspiking and the nearest prespiking was 6 ms. Closed circles indicate synaptic conductance in the allosteric model (average of three trials; SEM $<0.21\%$), and open circles indicate the correspondence in experiment (mean $\pm$ SEM) (Froemke et al., 2006) (***A–D***). ***C***, Changes of synaptic strength by postsynaptic bursts with a single presynaptic spike. The postspikes (with the indicated numbers) with 100 Hz together with a prespike were given at 1 Hz for 100 times, and synaptic conductance was plotted. The interval between the prespiking and the first postspiking was 6 ms. ***D***, Burst frequency-dependent synaptic plasticity. Five pairings of prespiking $\rightarrow$ postspiking (circles) and postspiking $\rightarrow$ prespiking (squares) with the indicated frequencies were given at 1 Hz for 100 times, and synaptic conductance was plotted (average of three trials; SEM $<0.26\%$).

imental result is consistent with the result of the allosteric model but not with that of the no-allosteric models. We confirmed that the allosteric model gives a better fit to the experimental data than the no-allosteric models by measuring $S(\theta, \Sigma)$, a sum of variance and covariance of mean squared errors between experiment and simulation in peak amplitude, peak time, and decay amplitude, normalized by the best-fit simulation (Fig. 5*F*). As $S(\theta, \Sigma)$ becomes closer to 1, the model fit improves. $S(\theta, \Sigma)$ of the allosteric model was closer to 1 than that of the no-allosteric models, regardless of the time constant. This indicates that the allosteric model gives a much better fit to the experimental data than the no-allosteric models. Therefore, only the allosteric model appears to be consistent with the experimental properties of NMDAR-EPSPs.

We also examined the robustness of the allosteric kinetics of NMDARs by measuring of goodness of fit against various time constants of $Ca^{2+} \cdot$CaM binding to NMDARs (Fig. 5*G*). We fixed τ_1 as 2.3 ms from the experimental NMDAR suppression (Fig. 3*C*) (Froemke et al., 2005) and changed τ_2 as indicated. We found that the allosteric kinetics can fit the NMDAR-EPSPs well in a wide range over 230 ms (100-fold difference between the time constants τ_1 and τ_2). In general, allosteric kinetics often accompanies a huge difference in time constants. For well-known allosteric kinetics of $Ca^{2+} \cdot$CaM binding to nonphosphorylated and phosphorylated CaMKII, the difference in time constants is ~1000-fold (supplemental information, available at http://www.kurodalab.org/info/STDP/Urakubo2008SI.pdf) (Meyer et al., 1992). Compared with such allosteric kinetics, a difference in time constants in the allosteric model of NMDARs (100-fold) is likely to be reasonable and physiological.

Complex spike train coding by the allosteric kinetics

We further tested the allosteric model with more complex spike patterns, shown previously to also induce STDP (Froemke and Dan, 2002; Wang et al., 2005; Froemke et al., 2006). We found that the allosteric model correctly predicted the direction of synaptic plasticity in spike triplet experiments (Fig. 6*A*,*B*) (supplemental Fig. 3, available at www.jneurosci.org as supplemental material) (Froemke and Dan, 2002), which indicated that the allosteric model can be extrapolated over STDP induced with more complex spike trains. We also validated the allosteric model with spike quadruplet experiments (Fig. 6*C*) (Froemke and Dan, 2002). We found a high correlation of the direction of synaptic plasticity between the allosteric model and the experiments (Fig. 6*C*) (Froemke and Dan, 2002). Finally, we validated the allosteric model using paired spike bursts instead of paired prespikes and postspikes (Fig. 7) (Froemke et al., 2006). The presynaptic burst after a postspike induced LTD at a similar extent, regardless of numbers of prespikes both in simulation and experiment (Fig. 7*A*). This is because of decreased probability of glutamate release during high-frequency stimulation (Tsodyks and Markram, 1997; Matveev and Wang, 2000) and of saturation of glutamate binding to NMDARs by a single prespike. The presynaptic burst before a postspike induced LTP, but the amplitude of LTP decreased as the number of prespikes increased (Fig. 7*B*). This is because a burst of five presynaptic spikes induced glutamate release mostly during the first or second spiking in the burst resulting from short-term depression; thereby the effective interval between prespiking and postspiking was prolonged, resulting in a reduction of the amplitude of LTP. The amplitudes of LTP with one or two prespikes in experiment are higher than those in the allosteric model because of the slower increase of LTP in the allosteric model; however, the amplitudes of LTP in experiment and the allosteric model became similar at longer periods (>60 min) (data not shown), which is in principle not inconsistent with the experimental data (Froemke et al., 2006). The postsynaptic burst with a single prespike induced a gradual shift from LTD to LTP as the number of postspikes increased both in experiment and in the allosteric model (Fig. 7*C*). The increase of the number of postspikes induced repetitive removal of the Mg^{2+} block from NMDARs, and this action overcame the suppres-

sion of NMDARs by Ca^{2+} · CaM, resulting in a gradual shift from LTD to LTP (Fig. 7*C*). The burst frequency-dependent synaptic plasticity was also similar between the experiments and the allosteric model (Fig. 7*D*) (Froemke et al., 2006). This result is consistent with the frequency-dependent synaptic plasticity at other synapses (Sjostrom et al., 2001). Therefore, the allosteric model appeared to be consistent with a wide range of complex spike train-dependent synaptic plasticity in layers II/III of visual cortex.

Requirement of postsynaptic NMDARs for the induction of LTD

We further compared the role of NMDARs in the induction of LTD between the allosteric model and the experimental results. Based on experiments, two NMDAR-dependent scenarios have been proposed for the induction of LTD by spike pairing. These two scenarios differ on the presumed synaptic location of NMDARs: one depends on activation of presynaptic NMDA autoreceptors (Sjostrom et al., 2003; Bender et al., 2006), and the other depends on postsynaptic NMDARs (Froemke et al., 2005; Seol et al., 2007). Therefore, we experimentally examined the requirement of postsynaptic NMDARs for the induction of LTD.

Through the recording electrodes, we loaded postsynaptic neurons with (+)-5-methyl-10,11-dihydro-5*H*-dibenzo [a,d] cyclohepten-5,10-imine maleate (MK-801) (1 mM), an NMDAR antagonist, and examined whether LTD could be induced (Fig. 8). Postspike → prespike pairing did not induce LTD in cells filled with MK-801 (change in EPSP slope, 5.6 ± 9.5%; $n = 3$; $p < 0.03$) but induced LTD in nearby cells (<30 μm; change in EPSP slope; −35.9 ± 9.0%), which were recorded at the same time, indicating that injection of MK-801 fully blocked the induction of LTD. We confirmed that intracellular MK-801 (1 mM) blocked NMDARs to the same degree as bath-applied AP-5 (50 μM); intracellular MK-801 reduced NMDAR-EPSP amplitude by −76.9 ± 5.5% ($n = 5$), whereas extracellular APV reduced NMDAR-EPSP amplitude by −80.2 ± 4.8% ($n = 4$; $p > 0.6$, compared with intracellular MK-801) in the presence of CNQX (20 μM) to block AMPARs and picrotoxin (10 μM) to block $GABA_A$ receptors. These results indicate that postsynaptic NMDARs are required for the induction of LTD and support our hypothesis that postsynaptic NMDARs are responsible for the induction of LTD at this synapse.

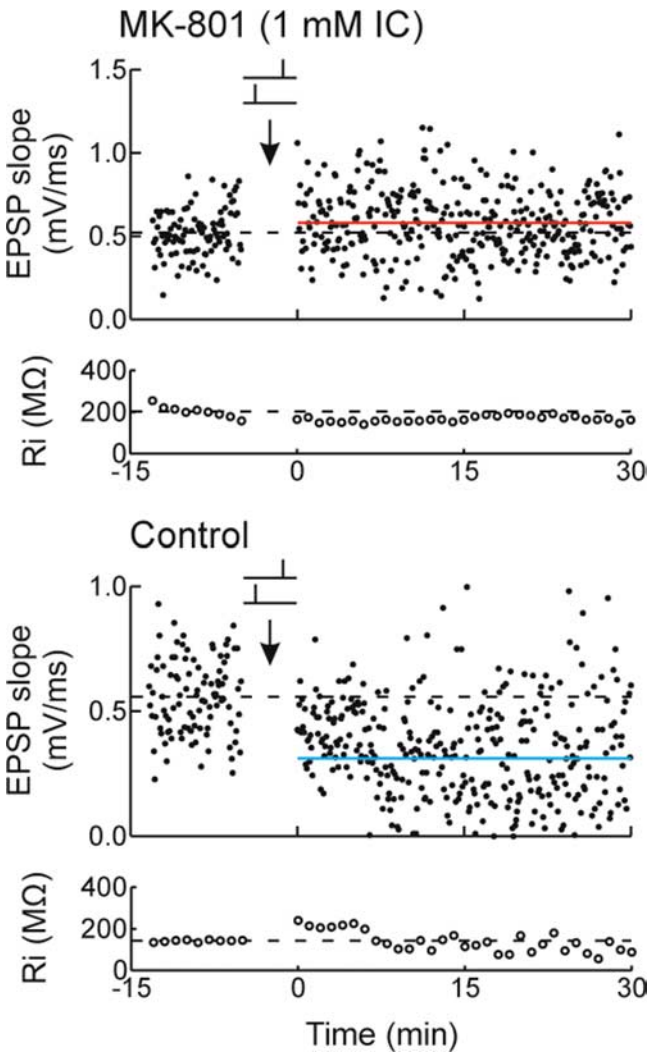

Figure 8. Requirement of postsynaptic NMDARs for the induction of LTD in STDP. Intracellular MK-801 (1 mM) prevented pairing-induced LTD. Examples of data from two simultaneously recorded neurons in the same slice are shown. Top, Recording with MK-801 in the internal solution. Bottom, Recording from a nearby neuron (~25 μm away). At the time indicated by the arrow, postspike → prespike pairing [$T_{post} - T_{pre} = -9.6$ ms (top), −10.3 ms (bottom)] was repeated. Red and blue lines indicate increase (11.8%; $p > 0.2$) and decrease (−44.8%; $p < 10^{-10}$) in synaptic strength. EPSP slope is shown in the top panel, and input resistance (R_i) is shown in the bottom panel.

Spike timing-dependent Ca^{2+} influx

Recent Ca^{2+} imaging experiments at a different synapse revealed that prespiking → postspiking triggered accelerated Ca^{2+} influx, whereas postspiking → prespiking did not show significant suppressed Ca^{2+} influx (Nevian and Sakmann, 2004). To investigate whether our model could reproduce this experimental result, we included in our simulation the presence of a Ca^{2+} indicator in the allosteric model (Fig. 9*A*). We found that suppression of Ca^{2+} influx (which was seen in the absence of the Ca^{2+} indicator) (Fig. 4*B*,*C*) was not triggered by postspiking → prespiking in the presence of the Ca^{2+} indicator. This is because rapid absorption of free Ca^{2+} by the Ca^{2+} indicator results in the reduction of Ca^{2+} binding to CaM, and the suppression of NMDARs by Ca^{2+} · CaM was not consequently triggered, resulting in disappearance of suppressed Ca^{2+} influx by postspiking → prespiking.

In addition, Ca^{2+} influx via NMDARs in the allosteric model seems to be far higher than Ca^{2+} influx via VGCCs, although some Ca^{2+}-imaging experiments have shown that Ca^{2+} influx via NMDARs is comparable with Ca^{2+} influx via VGCCs (Koester and Sakmann, 1998; Nevian and Sakmann, 2004) (Figs. 3*A*, 4*B*). This is simply because the observation site in the allosteric model was a PSD compartment, where NMDARs were highly concentrated, and the amplitudes of Ca^{2+} influx from NMDARs and VGCCs became comparable in the cytosol (Fig. 9*B*). Therefore, the ratio of Ca^{2+} influx via NMDARs and VGCCs is also consistent with the experimental results.

Extraction of an essential rule of STDP

We extracted a simple and essential learning rule by reduction of the allosteric model. The principle of Ca^{2+} influx in the allosteric model is that, with prespike → postspike timing, spiking prevents the suppression of NMDARs by Ca^{2+} · CaM via the allosteric kinetics of NMDARs, and postspiking triggers the removal of the Mg^{2+} block of NMDARs by depolarization of the postsynaptic membrane potential, resulting in accelerated Ca^{2+} influx and induction of LTP (Fig. 10*A*, left). In contrast, with postspike →

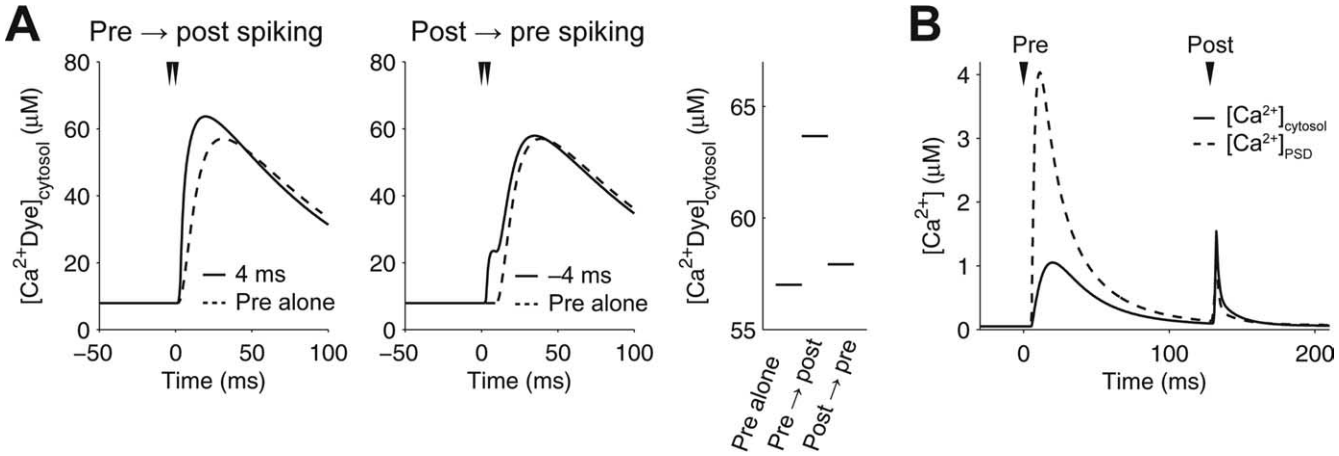

Figure 9. Spike timing-dependent Ca^{2+} influx. ***A***, Time courses of Ca^{2+}-bound Ca^{2+} indicator in cytosol (Conc, 100 μM; Kd, 580 nM) by prespiking → postspiking ($T_{post} - T_{pre} = 4$ ms; left) and postspiking → prespiking (−4 ms; center). Time courses of Ca^{2+}-bound Ca^{2+} indicator by a prespike alone were overlaid. Maximum of Ca^{2+}-bound Ca^{2+} indicator by prespiking, prespiking → postspiking and postspiking → prespiking are shown (right). ***B***, Time courses of $[Ca^{2+}]_{PSD}$ and $[Ca^{2+}]_{cytosol}$ by prespiking → postspiking with the indicated timing.

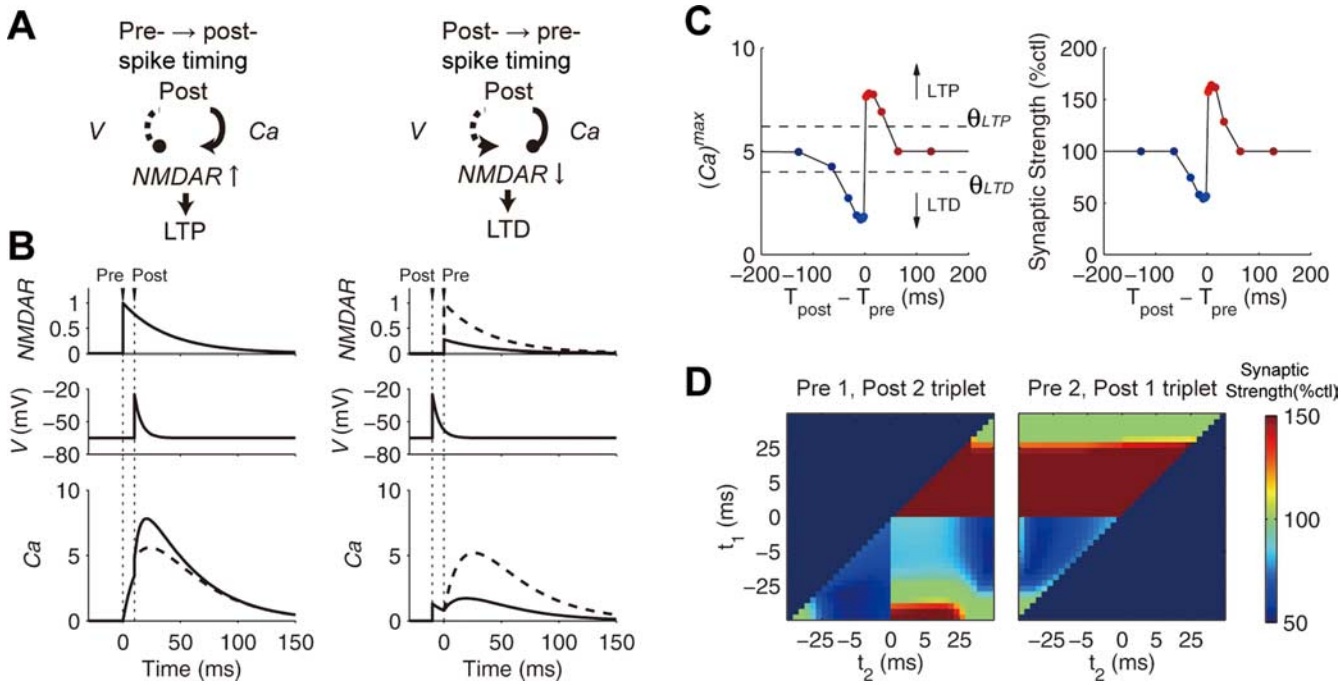

Figure 10. Simple STDP model. ***A***, The principle of STDP. Postspiking positively regulates NMDARs (*NMDAR*) via increase of membrane potential (*V*) with prespiking → postspike timing (left, solid line), resulting in induction of LTP (left). With this timing, Ca^{2+} · CaM (*Ca*) does not affect *NMDAR* via the allosteric kinetics (left, dashed line). Postspiking negatively regulates *NMDAR* via *Ca* with postspike → prespike timing (right, solid line), resulting in induction of LTD (right). With this timing, *V* does not effectively affect *NMDAR*, because *V* returns to the basal level when a prespike arrives (right, dashed line). ***B***, *NMDAR*(*t*), *V*(*t*), and *Ca*(*t*) by a single pairing of prespiking and postspiking with the indicated timing (Eqs. 1–3). The dashed line in *NMDAR* (top, right) indicates *NMDAR* with prespiking alone, and the dashed lines in *Ca* (bottom) indicate a linear sum of *Ca* induced by a prespike alone and a postspike alone with the indicated timing. ***C***, Spike timing-dependent *Ca* (left) and synaptic strength (right). The high and low *Ca* induced by a single pairing of prespiking and postspiking with the indicated timing were converted into LTP (above the threshold, θ_{LTP}) and LTD (below the threshold, θ_{LTD}), respectively (Eqs. 4, 5). ***D***, Synaptic plasticity induced with spike triplets. The relative spike timing of triplets, t_1 and t_2, is the same as in Figure 6.

prespike timing, postspiking triggers the suppression of NMDARs by Ca^{2+} · CaM via the allosteric kinetics of NMDARs, resulting in suppressed Ca^{2+} influx and induction of LTD (Fig. 10*A*, right). Note that increase of membrane potential by postspiking does not affect NMDARs with postspike → prespike timing, because membrane potential returns to the resting potential when prespiking arrives. Thus, postspiking positively and negatively regulates NMDAR activation via increase of membrane potential and suppression by Ca^{2+} · CaM, respectively. Based on this principle of the allosteric model, we write the simple STDP model as follows:

$$\frac{dNMDAR(t)}{dt} = -\frac{NMDAR(t)}{\tau_{NMDAR}}, \quad (1)$$

$$\frac{dV(t)}{dt} = -\frac{V(t) - V_{rest}}{\tau_V}, \quad (2)$$

$$\frac{dCa(t)}{dt} = NMDAR(t) \cdot (0.0223[V(t) - V_{rest}] + 0.05) - \frac{Ca(t)}{\tau_{Ca}}, \quad (3)$$

$$\text{if } t = t_{\text{post}} \text{ then } V(t) \rightarrow V(t) + AP,\ Ca(t) \rightarrow Ca(t) + Ca_{\text{VGCC}},$$
$$\text{if } t = t_{\text{pre}} \text{ then } NMDAR(t) \rightarrow NMDAR(t) + \frac{K_{\text{Ca}}}{K_{\text{Ca}} + Ca(t)}, \quad (4)$$

$$A_{\text{LTP/LTD}} = \begin{cases} A_{\text{LTP}} \cdot ([Ca(t)]^{\max} - \theta_{\text{LTP}}) & \theta_{\text{LTP}} < (Ca)^{\max} \\ 0 & \theta_{\text{LTD}} < (Ca)^{\max} \le \theta_{\text{LTP}} \\ A_{\text{LTD}} \cdot ([Ca(t)]^{\max} - \theta_{\text{LTD}}) & (Ca)^{\max} \le \theta_{\text{LTD}} \end{cases},$$
$$\text{Synaptic Strength} = 100 + A_{\text{LTP/LTD}}, \quad (5)$$

where $NMDAR(t)$, $V(t)$, and $Ca(t)$ represent NMDAR activity, membrane potential, and Ca^{2+} · CaM concentration, respectively; τ_{NMDAR}, τ_V, and τ_{Ca} are the decay time constants of $NMDAR(t)$, $V(t)$, and $Ca(t)$, respectively; V_{rest} is the resting membrane potential; AP is the amplitude of the backpropagating action potential; Ca_{VGCC} is the Ca^{2+} influx via VGCC; K_{Ca} is the effective Ca that gives the 50% inhibition of the maximal activity of $NMDAR$; t_{pre} and t_{post} are the timings of the prespiking and postspiking, respectively; $(Ca)^{\max}$ is the maximal value of Ca by a single pairing of prespiking and postspiking; θ_{LTP} and θ_{LTD} denote the thresholds of Ca for LTP and LTD, respectively; and A_{LTP}, A_{LTD}, and $A_{\text{LTP/LTD}}$ correspond to the amplitudes of LTP, LTD, and consequent synaptic strength, respectively. We set $\tau_{\text{NMDAR}} = 40$ ms, $\tau_V = 6$ ms, $\tau_{\text{Ca}} = 20$ ms, $V_{\text{rest}} = -65$ mV, $AP = 40$ mV, $Ca_{\text{VGCC}} = 1.3$, $K_{\text{Ca}} = 0.3$, $\theta_{\text{LTP}} = 6.2$, $\theta_{\text{LTD}} = 4$, $A_{\text{LTP}} = 40$, and $A_{\text{LTD}} = 20$.

Equations 1 and 2 represent the decays of NMDAR activity and membrane potential, respectively. Equation 3 represents that Ca^{2+} increase depends on the voltage-dependent activation of NMDARs with an exponential decay, where $(0.0223[V(t) - V_{\text{rest}}] + 0.5)$ denotes the voltage dependence of NMDARs, which is obtained by the linearization of the voltage dependence of NMDARs in the allosteric model around the resting membrane potential (supplemental information, available at http://www.kurodalab.org/info/STDP/Urakubo2008SI.pdf). In Equation 4, at $t = t_{\text{post}}$, postspiking triggers the increase of voltage via bpAP and Ca^{2+} increase via VGCC, whereas at $t = t_{\text{pre}}$, $NMDAR$ is activated in a reciprocal manner of Ca. Equations 3 and 4 indicate that Ca acts on $NMDAR$ only at $t = t_{\text{pre}}$ but not later, which means that the suppression of NMDARs reflects Ca^{2+} level at prespiking but not after prespiking. Therefore, Equations 3 and 4 represent the allosteric kinetics of NMDARs. The difference in Equation 4 used when $t = t_{\text{pre}}$ and $t = t_{\text{post}}$ enables LTP induction with the prespike → postspike timing and LTD induction with the postspike → prespike timing. Equation 5 represents that the high Ca^{2+} influx results in LTP via CaMKII, and the low Ca^{2+} influx results in LTD via PP1.

The high and low Ca were induced with the prespike → postspike and the postspike → prespike timing, respectively (Fig. 10*B*). With the prespike → postspike timing, $NMDAR$ is fully activated because of the absence of Ca at $t = t_{\text{pre}}$, whereas with the postspike → prespike timing, $NMDAR$ is weakly activated because of the presence of Ca at $t = t_{\text{pre}}$ (Fig. 10*B*) (Eq. 3). This dependence of $NMDAR$ on Ca at $t = t_{\text{pre}}$ clearly indicates that the intracellular Ca^{2+} concentration, when NMDARs are activated, carries the previous prespike and postspike-timing information. The simple STDP model was capable of reproducing the spike timing-dependent Ca (Fig. 10*C*, left) and consequent STDP (Fig. 10*C*, right). Note that the high and low Ca, but not moderate one, triggered LTP and LTD, respectively. The time window for LTP depends on the decay time constant of NMDARs, and that for LTD on the decay time constant of Ca^{2+} increase by VGCC, which are consistent with the allosteric model. Synaptic plasticity induced by spike triplets was coherently reproduced (Fig. 10*D*). These results were similar to those in the allosteric model (Figs. 4*B–E*, 6*A*,*B*), indicating that the simple STDP model retains the essential properties of the allosteric model. Thus, the bidirectional role of postspiking via the allosteric kinetics of NMDARs in STDP, rather than the detailed parameters and complicated molecular interactions, is the essential principle of STDP.

Discussion

We show that the simple allosteric kinetics of NMDARs codes complex spike-timing information into STDP. The allosteric kinetics of NMDARs depends on the different time constants of Ca^{2+} · CaM to glutamate-bound and glutamate-unbound NMDARs. In general, the allosteric kinetics accompanies the changes of affinity, and it is possible that the allosteric kinetics of NMDARs also accompanies the changes of Ca^{2+} · CaM affinity for glutamate-bound and glutamate-unbound NMDARs. Similar results were obtained if the affinity of glutamate for Ca^{2+} · CaM-unbound NMDARs were over four times higher than that for Ca^{2+} · CaM-bound NMDARs (data not shown), although the affinity of glutamate to NMDARs is not significantly affected by binding Ca^{2+} · CaM to NMDARs (Zhang et al., 1998). The principle of our prediction is that any similar allosteric kinetics of NMDARs that depends on the timing between prespiking and postspiking can account for STDP, even if STDP is Ca^{2+} · CaM independent. Taking into consideration that STDP has been experimentally observed across a wide range of preparations, a single molecular property, such as an allosteric kinetics of NMDARs, seems more reasonable to account for STDP, rather than other complex molecular events, such as phosphorylation/dephosphorylation, because the former is more robust against variable expression levels of molecules.

CaN is required to suppress NMDARs with postspiking → prespiking (Froemke et al., 2005). Phosphatase activity of CaN is not likely to detect such short timing simply because Ca^{2+}-dependent activation of phosphatase activity of CaN requires a longer time constant (Klee et al., 1998). In addition, dephosphorylation of NMDARs by CaN or other related phosphatases was required to associate Ca^{2+} · CaM to the NMDARs (Rycroft and Gibb, 2004a). Therefore, CaN activity may be a prerequisite condition for detecting the postspiking → prespiking, such as dephosphorylation of NMDARs, and this is implicitly incorporated into NMDAR kinetics in the allosteric model.

Although particular detailed parameters of our model may be unsupported by experimental observations, our main conclusion in this study is the bidirectional role of postspiking based on the allosteric kinetics of NMDARs in STDP as shown by the model reduction, and this does not critically depend on the exact details of most of the parameters. We emphasize that the signaling cascades in the allosteric model should be regarded as a tentative description, rather than a complete description. For example, some signaling cascades in the allosteric model, such as PP1, are based on the previous reports in other types of synaptic plasticity such as LTD induced by prolonged low-frequency presynaptic stimulation (LFS) (Mulkey et al., 1993), but they have not been shown to be directly involved in STDP. Also, in the allosteric model, LTP induced by high-frequency presynaptic stimulation,

but not LTD induced by prolonged LFS (typically 900 times at 1 Hz), could be reproduced (data not shown) (Bear and Malenka, 1994). This implies the possibility that a missing pathway, requiring a long duration of the stimulus (>10 min), may be responsible for LTD induced by prolonged LFS. Note that 100 prespikes at 1 Hz alone did not induce LTD both in simulation and experiment (Fig. 4*E*) (Mizuno et al., 2001; Johnston et al., 2003). Additionally, another class of STDP has been shown to involve a distinct form of LTD that is independent of postsynaptic NMDARs and may be presynaptically expressed (Sjostrom et al., 2003; Bender et al., 2006). The STDP in layer II/III of visual cortex is not consistent with doublet-dependent STDP (Wittenberg and Wang, 2006) and triplet-dependent STDP (Wang et al., 2005) in hippocampal CA1 neurons. This suggests the possibility of requirement of an additional pathway(s) for the STDP in hippocampal CA1 neurons. The extension of the model by incorporating the future progress will shed light on the general principles of distinct classes of STDP.

A recent study reported that NMDAR subtypes are selective for the direction of synaptic modification in STDP (Gerkin et al., 2007). Our results indicate that the kinetics of NMDARs should detect the interaction between prespiking and postspiking. Together, the selectivity of NMDAR subtypes for the direction of synaptic modification may be attributable to the subtype-dependent different kinetics of NMDARs in Ca^{2+} · CaM binding or in the voltage dependence, both of which can be considered part of the postspiking signal.

Several biophysical models of STDP have been proposed in which postsynaptic Ca^{2+} influx also serves as a spike-timing detector (Karmarkar and Buonomano, 2002; Shouval et al., 2002; Rubin et al., 2005). These models assume that the basal Ca^{2+} influx induced by uncorrelated prespiking and postspiking (less than −200 or >100 ms) is far lower than that for LTD and LTP, and the postspiking → prespiking induces moderate Ca^{2+} influx for LTD, whereas the prespiking → postspiking induces high Ca^{2+} influx for LTP. However, with this assumption, it is difficult to avoid unnecessary LTD induction by the prespiking → postspiking with a long interval, which has not usually been observed in experiments (Sjostrom and Nelson, 2002), although some modifications have been proposed to avoid this (Rubin et al., 2005; Shouval and Kalantzis, 2005). Also, a biophysical model has been proposed to explain synaptic plasticity induced by spike triplets (Shah et al., 2006). However, this model uses the unnecessary LTD induction by the prespiking → postspiking to explain synaptic plasticity induced by spike triplets. In contrast, in the allosteric model, we set that the prespiking → postspiking, the uncorrelated spiking, and the postspiking → prespiking induced the high, moderate, and low Ca^{2+} influx, which led to potentiation, no change (neither potentiation nor depression), and depression, respectively (Koester and Sakmann, 1998; Cho et al., 2001; Lisman, 2001; Froemke et al., 2005) (Fig. 10*C*) (supplemental Fig. 4, available at www.jneurosci.org as supplemental material). This makes the allosteric model free from the unnecessary induction of LTD by the prespiking → postspiking, regardless of timing interval, and the allosteric model can coherently explain synaptic plasticity induced by a variety of complex spike trains within a single framework. Additionally, we experimentally found that the partial blockage of NMDAR activity induces depression, and the facilitation of NMDAR activity with removal of Mg^{2+} induces potentiation (supplemental Fig. 1, available at www.jneurosci.org as supplemental material). The biphasic synaptic modification against NMDAR activity is consistent with the hypothesis of the three Ca^{2+} levels for synaptic plasticity, because Ca^{2+} influx dominantly depends on NMDARs. Together, the three Ca^{2+} levels for synaptic plasticity is substantially evident from both phenomenological experiments (synaptic plasticity induced by spike doublets, spike triplets, and more complex spike trains) and pharmacological experiments (supplemental Fig. 1, available at www.jneurosci.org as supplemental material).

Our allosteric model belongs to the one-coincidence detector model. A model of two-coincidence detectors for STDP has also been proposed (Karmarkar and Buonomano, 2002). In the model, voltage-dependent Mg^{2+} removal from NMDARs detects prespiking → postspiking for LTP, whereas metabotropic GluRs (mGluRs) and Ca^{2+} influx via VGCCs detects postspiking → prespiking for LTD. Recently, some experiments have revealed that such secondary coincidence detectors are involved in LTD of STDP at other synapses: mGluRs at synapses between layer IV and layer II/III neurons in the somatosensory cortex (Bender et al., 2006) and CB_1 receptors at synaptic connections between layer V pyramidal cells (Sjostrom et al., 2003). Taking our findings of requirement of rapid suppression by postspiking into consideration, these molecules should interact with a postspiking signal with the time constant on an order of a few ten milliseconds. Such rapid time constant may depend on the ion flux or changes of voltage, rather than phosphorylation/dephosphorylation processes or catalytic activities of downstream of mGluR1 and CB_1 receptors.

We analyzed the sensitivity of the amplitude of STDP against the conductance of AMPARs, because the amplitude of LTP in STDP has been reported to be dependent on the size of the initial EPSPs (Bi and Poo, 1998; Sjostrom et al., 2001), which depends on the AMPAR activity, and this issue is theoretically related to the boundary condition on synaptic plasticity, whether the changes of synaptic strength depend on the current synaptic weight or not (Song et al., 2000; van Rossum et al., 2000; Cateau and Fukai, 2003). The relative amplitudes of LTP induced by prespiking → postspiking remained the same against the changes of conductance of AMPARs (supplemental Fig. 5, available at www.jneurosci.org as supplemental material). This means that the amplitude of LTP is positively correlated with the size of the initial EPSPs, which is similar to the theoretical study of the multiplicative learning rule (van Rossum et al., 2000; Cateau and Fukai, 2003). However, additional experimental studies are necessary to conclude this issue.

In conclusion, the allosteric model appears to be consistent with specific features of STDP, such as spike timing-dependent NMDAR-EPSPs and spike doublet-, triplet-, quadruplet-, and burst-dependent synaptic plasticity within a single framework. This study provides a novel concept of the bidirectional role of postspiking in induction of synaptic plasticity by the allosteric kinetics of NMDARs.

References

Artola A, Brocher S, Singer W (1990) Different voltage-dependent thresholds for inducing long-term depression and long-term potentiation in slices of rat visual cortex. Nature 347:69–72.

Bear MF, Malenka RC (1994) Synaptic plasticity: LTP and LTD. Curr Opin Neurobiol 4:389–399.

Bender VA, Bender KJ, Brasier DJ, Feldman DE (2006) Two coincidence detectors for spike timing-dependent plasticity in somatosensory cortex. J Neurosci 26:4166–4177.

Bhalla US, Iyengar R (1999) Emergent properties of networks of biological signaling pathways. Science 283:381–387.

Bi GQ, Poo MM (1998) Synaptic modifications in cultured hippocampal neurons: dependence on spike timing, synaptic strength, and postsynaptic cell type. J Neurosci 18:10464–10472.
Bi GQ, Poo MM (2001) Synaptic modification by correlated activity: Hebb's postulate revisited. Annu Rev Neurosci 24:139–166.
Bi GQ, Rubin J (2005) Timing in synaptic plasticity: from detection to integration. Trends Neurosci 28:222–228.
Blitzer RD, Connor JH, Brown GP, Wong T, Shenolikar S, Iyengar R, Landau EM (1998) Gating of CaMKII by cAMP-regulated protein phosphatase activity during LTP. Science 280:1940–1942.
Boettiger CA, Doupe AJ (2001) Developmentally restricted synaptic plasticity in a songbird nucleus required for song learning. Neuron 31:809–818.
Cateau H, Fukai T (2003) A stochastic method to predict the consequence of arbitrary forms of spike-timing-dependent plasticity. Neural Comput 15:597–620.
Cho K, Aggleton JP, Brown MW, Bashir ZI (2001) An experimental test of the role of postsynaptic calcium levels in determining synaptic strength using perirhinal cortex of rat. J Physiol (Lond) 532:459–466.
Collingridge GL, Isaac JT, Wang YT (2004) Receptor trafficking and synaptic plasticity. Nat Rev Neurosci 5:952–962.
Corlew R, Wang Y, Ghermazien H, Erisir A, Philpot BD (2007) Developmental switch in the contribution of presynaptic and postsynaptic NMDA receptors to long-term depression. J Neurosci 27:9835–9845.
Dan Y, Poo MM (2004) Spike timing-dependent plasticity of neural circuits. Neuron 44:23–30.
Doi T, Kuroda S, Michikawa T, Kawato M (2005) Inositol 1,4,5-trisphosphate-dependent Ca^{2+} threshold dynamics detect spike timing in cerebellar Purkinje cells. J Neurosci 25:950–961.
Ehlers MD, Zhang S, Bernhadt JP, Huganir RL (1996) Inactivation of NMDA receptors by direct interaction of calmodulin with the NR1 subunit. Cell 84:745–755.
Feldman DE (2000) Timing-based LTP and LTD at vertical inputs to layer II/III pyramidal cells in rat barrel cortex. Neuron 27:45–56.
Froemke RC, Dan Y (2002) Spike-timing-dependent synaptic modification induced by natural spike trains. Nature 416:433–438.
Froemke RC, Poo MM, Dan Y (2005) Spike-timing-dependent synaptic plasticity depends on dendritic location. Nature 434:221–225.
Froemke RC, Tsay IA, Raad M, Long JD, Dan Y (2006) Contribution of individual spikes in burst-induced long-term synaptic modification. J Neurophysiol 95:1620–1629.
Gallant AR (1987) Multivariate nonlinear regression. In: Nonlinear statistical models, pp 267–404. New York: Wiley.
Gerkin RC, Lau PM, Nauen DW, Wang YT, Bi GQ (2007) Modular competition driven by NMDA receptor subtypes in spike-timing-dependent plasticity. J Neurophysiol 97:2851–2862.
Gerstner W, Kempter R, van Hemmen JL, Wagner H (1996) A neuronal learning rule for sub-millisecond temporal coding. Nature 383:76–81.
Hayer A, Bhalla US (2005) Molecular switches at the synapse emerge from receptor and kinase traffic. PLoS Comput Biol 1:137–154.
Hoffman DA, Magee JC, Colbert CM, Johnston D (1997) K^+ channel regulation of signal propagation in dendrites of hippocampal pyramidal neurons. Nature 387:869–875.
Johnston D, Christie BR, Frick A, Gray R, Hoffman DA, Schexnayder LK, Watanabe S, Yuan LL (2003) Active dendrites, potassium channels and synaptic plasticity. Philos Trans R Soc Lond B Biol Sci 358:667–674.
Kampa BM, Clements J, Jonas P, Stuart GJ (2004) Kinetics of Mg^{2+} unblock of NMDA receptors: implications for spike-timing dependent synaptic plasticity. J Physiol (Lond) 556:337–345.
Karmarkar UR, Buonomano DV (2002) A model of spike-timing dependent plasticity: one or two coincidence detectors? J Neurophysiol 88:507–513.
Klee CB, Ren H, Wang X (1998) Regulation of the calmodulin-stimulated protein phosphatase, calcineurin. J Biol Chem 273:13367–13370.
Koester HJ, Sakmann B (1998) Calcium dynamics in single spines during coincident pre- and postsynaptic activity depend on relative timing of back-propagating action potentials and subthreshold excitatory postsynaptic potentials. Proc Natl Acad Sci USA 95:9596–9601.
Kuroda S, Schweighofer N, Kawato M (2001) Exploration of signal transduction pathways in cerebellar long-term depression by kinetic simulation. J Neurosci 21:5693–5702.
Lisman J (1989) A mechanism for the Hebb and the anti-Hebb processes underlying learning and memory. Proc Natl Acad Sci USA 86:9574–9578.
Lisman J, Schulman H, Cline H (2002) The molecular basis of CaMKII function in synaptic and behavioural memory. Nat Rev Neurosci 3:175–190.
Lisman JE (2001) Three Ca^{2+} levels affect plasticity differently: the LTP zone, the LTD zone and no man's land. J Physiol (Lond) 532:285.
Malenka RC, Bear MF (2004) LTP and LTD: an embarrassment of riches. Neuron 44:5–21.
Malinow R, Malenka RC (2002) AMPA receptor trafficking and synaptic plasticity. Annu Rev Neurosci 25:103–126.
Matveev V, Wang XJ (2000) Implications of all-or-none synaptic transmission and short-term depression beyond vesicle depletion: a computational study. J Neurosci 20:1575–1588.
Meyer T, Hanson PI, Stryer L, Schulman H (1992) Calmodulin trapping by calcium-calmodulin-dependent protein kinase. Science 256:1199–1202.
Migliore M, Hoffman DA, Magee JC, Johnston D (1999) Role of an A-type K^+ conductance in the back-propagation of action potentials in the dendrites of hippocampal pyramidal neurons. J Comput Neurosci 7:5–15.
Mizuno T, Kanazawa I, Sakurai M (2001) Differential induction of LTP and LTD is not determined solely by instantaneous calcium concentration: an essential involvement of a temporal factor. Eur J Neurosci 14:701–708.
Mu Y, Poo MM (2006) Spike timing-dependent LTP/LTD mediates visual experience-dependent plasticity in a developing retinotectal system. Neuron 50:115–125.
Mulkey RM, Herron CE, Malenka RC (1993) An essential role for protein phosphatases in hippocampal long-term depression. Science 261:1051–1055.
Nevian T, Sakmann B (2004) Single spine Ca^{2+} signals evoked by coincident EPSPs and backpropagating action potentials in spiny stellate cells of layer 4 in the juvenile rat somatosensory barrel cortex. J Neurosci 24:1689–1699.
Pfister JP, Gerstner W (2006) Triplets of spikes in a model of spike timing-dependent plasticity. J Neurosci 26:9673–9682.
Poirazi P, Brannon T, Mel BW (2003) Arithmetic of subthreshold synaptic summation in a model CA1 pyramidal cell. Neuron 37:977–987.
Rubin JE, Gerkin RC, Bi GQ, Chow CC (2005) Calcium time course as a signal for spike-timing-dependent plasticity. J Neurophysiol 93:2600–2613.
Rycroft BK, Gibb AJ (2002) Direct effects of calmodulin on NMDA receptor single-channel gating in rat hippocampal granule cells. J Neurosci 22:8860–8868.
Rycroft BK, Gibb AJ (2004a) Inhibitory interactions of calcineurin (phosphatase 2B) and calmodulin on rat hippocampal NMDA receptors. Neuropharmacology 47:505–514.
Rycroft BK, Gibb AJ (2004b) Regulation of single NMDA receptor channel activity by alpha-actinin and calmodulin in rat hippocampal granule cells. J Physiol (Lond) 557:795–808.
Sabatini BL, Maravall M, Svoboda K (2001) Ca^{2+} signaling in dendritic spines. Curr Opin Neurobiol 11:349–356.
Senn W (2002) Beyond spike timing: the role of nonlinear plasticity and unreliable synapses. Biol Cybern 87:344–355.
Seol GH, Ziburkus J, Huang S, Song L, Kim IT, Takamiya K, Huganir RL, Lee HK, Kirkwood A (2007) Neuromodulators control the polarity of spike-timing-dependent synaptic plasticity. Neuron 55:919–929.
Shah NT, Yeung LC, Cooper LN, Cai Y, Shouval HZ (2006) A biophysical basis for the inter-spike interaction of spike-timing-dependent plasticity. Biol Cybern 95:113–121.
Shouval HZ (2005) Clusters of interacting receptors can stabilize synaptic efficacies. Proc Natl Acad Sci USA 102:14440–14445.
Shouval HZ, Kalantzis G (2005) Stochastic properties of synaptic transmission affect the shape of spike time-dependent plasticity curves. J Neurophysiol 93:1069–1073.
Shouval HZ, Bear MF, Cooper LN (2002) A unified model of NMDA receptor-dependent bidirectional synaptic plasticity. Proc Natl Acad Sci USA 99:10831–10836.
Sjostrom PJ, Nelson SB (2002) Spike timing, calcium signals and synaptic plasticity. Curr Opin Neurobiol 12:305–314.
Sjostrom PJ, Turrigiano GG, Nelson SB (2001) Rate, timing, and cooperativity jointly determine cortical synaptic plasticity. Neuron 32:1149–1164.
Sjostrom PJ, Turrigiano GG, Nelson SB (2003) Neocortical LTD via coinci-

dent activation of presynaptic NMDA and cannabinoid receptors. Neuron 39:641–654.

Song S, Miller KD, Abbott LF (2000) Competitive Hebbian learning through spike-timing-dependent synaptic plasticity. Nat Neurosci 3:919–926.

Stiefel KM, Tennigkeit F, Singer W (2005) Synaptic plasticity in the absence of backpropagating spikes of layer II inputs to layer V pyramidal cells in rat visual cortex. Eur J Neurosci 21:2605–2610.

Stuart GJ, Hausser M (2001) Dendritic coincidence detection of EPSPs and action potentials. Nat Neurosci 4:63–71.

Tsodyks MV, Markram H (1997) The neural code between neocortical pyramidal neurons depends on neurotransmitter release probability. Proc Natl Acad Sci USA 94:719–723.

Tzounopoulos T, Kim Y, Oertel D, Trussell LO (2004) Cell-specific, spike timing-dependent plasticities in the dorsal cochlear nucleus. Nat Neurosci 7:719–725.

van Rossum MC, Bi GQ, Turrigiano GG (2000) Stable Hebbian learning from spike timing-dependent plasticity. J Neurosci 20:8812–8821.

Vislay-Meltzer RL, Kampff AR, Engert F (2006) Spatiotemporal specificity of neuronal activity directs the modification of receptive fields in the developing retinotectal system. Neuron 50:101–114.

Wang HX, Gerkin RC, Nauen DW, Bi GQ (2005) Coactivation and timing-dependent integration of synaptic potentiation and depression. Nat Neurosci 8:187–193.

Winder DG, Sweatt JD (2001) Roles of serine/threonine phosphatases in hippocampal synaptic plasticity. Nat Rev Neurosci 2:461–474.

Wittenberg GM, Wang SS (2006) Malleability of spike-timing-dependent plasticity at the CA3-CA1 synapse. J Neurosci 26:6610–6617.

Zhang S, Ehlers MD, Bernhardt JP, Su CT, Huganir RL (1998) Calmodulin mediates calcium-dependent inactivation of *N*-methyl-D-aspartate receptors. Neuron 21:443–453.